Energy & Environmental Science

Accepted Manuscript

ROYAL SOCIETY OF CHEMISTRY

www.rsc.org/ees

Journal Name

ARTICLE

Simple molecular structure and efficient triazine-based interfacial layer for high performance organic electronics†

Received 00th January 20xx,
Accepted 00th January 20xx

DOI: 10.1039/x0xx00000x

www.rsc.org/

Nallan Chakravarthi,[a] Kumarasamy Gunasekar,[a] Woosum Cho,[a] Dang Xuan Long,[b] Yun-Hi Kim,[c] Chang Eun Song,[d] Jong-Cheol Lee,[d] Antonio Facchetti,[e] Myungkwan Song,*[f] Yong-Young Noh*[b] and Sung-Ho Jin*[a]

Enabling state-of-the-art performance for solution processable and flexible organic electronics requires efficient, stable, and cost-effective interfacial layers (ILs). Here, we report an alcohol soluble phosphine oxide functionalized 1,3,5-triazine derivative (PO-TAZ) as an IL, that remarkably tailors the work function of conductors including metals, transparent metal oxides and organic materials which makes it an ideal candidate for an interfacial material in organic electronics. Consequently, PO-TAZ thin films enable organic and organic-inorganic (perovskite) solar cells with power conversion efficiencies of 10.04% and 16.41%, respectively, and n-channel organic field-effect transistors with electron mobility of 8 $cm^2\ V^{-1}\ s^{-1}$. Owing to the low-cost processing associated with PO-TAZ and the tremendous improvement in device performances as compared to the devices without PO-TAZ along with ambient stability, PO-TAZ is a good prospect for efficient organic electronics in large area printing processes.

1. Introduction

To facilitate electron injection/extraction in modern optoelectronic devices, the incorporation of interfacial layers on air-stable metal electrodes has been widely used.[1-3] The appropriate choice of interface materials provides a platform to precisely regulate the electrode work function (ϕ), protect the semiconductor layer from the diffusion of metals, and mitigate charge accumulation and recombination at the electrodes.[4,5] Various materials, such as CsF, LiF, Cs_2CO_3,[6] conjugated,[7] and non-conjugated polyelectrolytes,[8] and fullerene derivatives[9,10] have been utilized for improving electron injection/extraction properties. However, several challenges remain to overcome for the affordable use of interfacial layer (IL) in printed and large-area devices, such as low chemical and ambient stability, intricate synthetic and purification methodologies, poor batch-to-batch reproducibility, and high vacuum-based expensive film deposition processes. Here, we report a solution-processable phosphine oxide (P=O) functionalized 1,3,5-triazine derivative [PO-TAZ, 2-(3-(diphenylphosphoryl)-2,4-difluorophenyl)-4,6-diphenoxy-1,3,5-triazine)] as an effective IL in organic solar cells (OSCs), perovskite solar cells (PSCs), and n-channel organic field-effect transistors (OFETs). PO-TAZ is a very simple structured organic small molecule (**Fig. 1a**) synthesized by a simple protocol with inexpensive 2,4,6-trichloro-1,3,5-triazine (cyanuric chloride) as a starting material. PO-TAZ possesses good solubility in environmentally friendly solvents, e.g., alcohols, owing to the presence of a polar P=O group, ensuring compatibility with large-area printing process. Pioneering studies showed that the P=O functional group remarkably reduces the ϕ of Al and Ag by formation of an interfacial dipole at the semiconductor/electrode interface.[11,12] In addition, 1,3,5-triazine-based compounds are well known as efficient electron transport layers in organic light-emitting diodes.[13] Thus, PO-TAZ was designed combing the functions of both the P=O and 1,3,5-triazine moieties and is expected to facilitate electron injection/extraction in organic electronics. The detailed synthetic scheme, procedures, ^{1}H NMR of PO-TAZ, absorption spectra and thermal gravimetric analysis are provided in the Supplementary Information (**Fig. S1a** and **S2**, ESI†). It is noteworthy to acknowledge that pure PO-TAZ is readily obtained by simple column chromatography technique, which demonstrates more potential than fullerene derivatives and polymer-based interlayer materials, which require intricate synthesis and purification methods. Furthermore, the purification of PO-TAZ via train sublimation technique also

[a] Department of Chemistry Education, Graduate Department of Chemical Materials, and Institute for Plastic Information and Energy Materials, Pusan National University, Busan, 609-735, Republic of Korea. Email: shjin@pusan.ac.kr
[b] Department of Energy and Materials Engineering, Dongguk University, Seoul 100-715, Republic of Korea. Email: ynoh@dongguk.edu
[c] Department of Chemistry, Gyeongsang National University, Jinju 660-701, Republic of Korea
[d] Energy Materials Research Center, Korea Research Institute of Chemical Technology (KRICT), Daejeon 305-343, Republic of Korea
[e] OPV Group, Polyera Corporation, IL 60077, USA
[f] Surface Technology Division, Korea Institute of Materials Science, Changwon 641-831, Republic of Korea. Email: smk1017@kims.re.kr

† Electronic Supplementary Information (ESI) available: Experimental details, device fabrication method for OSCs, PSCs and OFETs, TGA and ^{1}H NMR of PO-TAZ. See DOI: 10.1039/x0xx00000x

Journal Name

ARTICLE

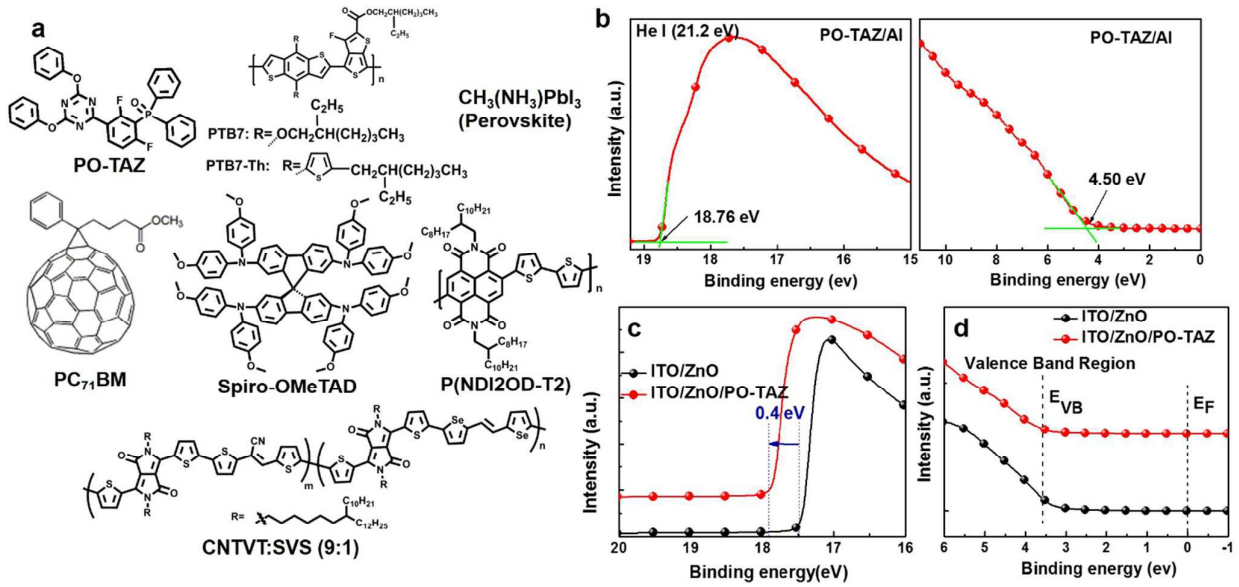

Fig. 1 (a) Structures of PO-TAZ, polymer donors, acceptor, hole transporting material, perovskite, and semiconducting polymers used for n-channel OFETs; (b) UPS spectra of PO-TAZ on Al; (c) secondary cut-off UPS spectra for glass/ITO/ZnO and glass/ITO/ZnO/PO-TAZ; (d) valence band region spectra for glass/ITO/ZnO and glass/ITO/ZnO/PO-TAZ.

proved the compatibility of PO-TAZ for vacuum deposition technique.

2. Results and discussion

2.1. Synthesis of PO-TAZ and photoelectron spectroscopy measurements

PO-TAZ was synthesized as shown in **Fig. S1a**, ESI†: the intermediate 1 (2-chloro-4,6-diphenoxy-1,3,5-triazine) was prepared from the reaction between cyanuric chloride and phenol in the presence of sodium hydroxide. Then, the chlorine-substituted 1,3,5-triazine unit was coupled with 2,4-difluorobenzeneboronic acid using a palladium-catalyzed cross-coupling reaction to give intermediate 2. Finally, PO-TAZ was obtained in a three-step process: regioselective lithiation of intermediate 2, coupling with chlorodiphenylphosphine, and oxidation with hydrogen peroxide. The thermal stability of PO-TAZ was found to be over 300 °C (**Fig. S1b**, ESI†) and the optical band gap (E_g^{opt}) of PO-TAZ was measured to be 3.99 eV (**Fig. S1c**, ESI†). The highest occupied molecular orbital (HOMO) of PO-TAZ was measured by ultraviolet photoelectron spectroscopy (UPS) and found to be -6.96 eV (**Fig. 1b**) and the lowest unoccupied molecular orbital (LUMO) energy level of PO-TAZ was calculated to be −2.97 eV from E_g^{opt} and HOMO. The deep HOMO level for PO-TAZ is due to the presence of 1,3,5-triazine unit[14] in the molecular structure of PO-TAZ. Additionally, the study of X-ray photoelectron spectroscopy core level spectra (**Fig. S3**, ESI†) of PO-TAZ film on Al shows the interaction at the interface between PO-TAZ and Al (coupling between P=O and Al). The UPS spectra (**Fig. S4**, ESI†) of PO-TAZ on ITO displayed a shift in ϕ from 4.4 to 2.68 eV, indicating the formation of an interfacial dipole. Additionally, as a further evidence of the effect of PO-TAZ, the photoemission onset of a ZnO film on ITO shifts towards the higher energy direction upon the deposition of PO-TAZ (**Fig. 1c**), whereas no shift was seen in the valence band region after introduction of the PO-TAZ (**Fig. 1d**). **Fig. 2a** shows PO-TAZ as an insulating layer in both conventional OSC and inverted OSC (IOSC) with LUMO level at −2.97 eV. The interfacial dipole between the electrode and the PO-TAZ layer in OSC, as well in ZnO and the PO-TAZ layer in IOSC is responsible for the observed improvement in charge carrier injection. Due to the shift in the vacuum level in solid state, the energy barrier for electron injection and collection could be reduced, as shown schematically in **Fig. 2b**. The ϕ lowering would also result in increasing the built-in potential (V_{BI}) in conventional OSC and IOSC devices, thus facilitating the electron extraction.

Journal Name

ARTICLE

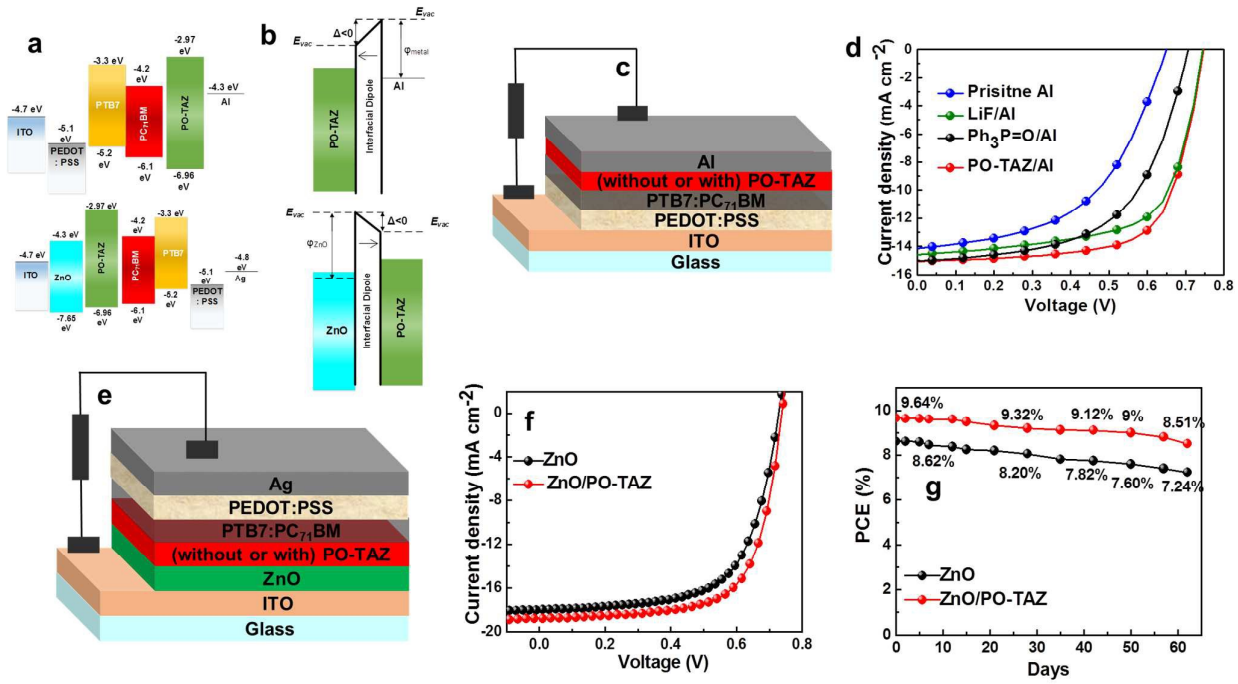

Fig. 2 (a) Proposed energy level diagrams of conventional and inverted OSCs; (b) schematic energy diagram of an interfacial dipole formed due to PO-TAZ in conventional and inverted OSCs; (c) device structure of conventional OSCs; (d) *J–V* curves of conventional OSCs with or without PO-TAZ; (e) device structure of inverted OSCs; (f) *J–V* curves of inverted OSCs with or without PO-TAZ; (g) long-term stability curves of inverted OSCs for a period of 60 days.

2.2. Conventional organic solar cells

Solution-processed conventional OSCs were fabricated using PO-TAZ as IL with a bulk heterojunction (BHJ) photoactive layer containing a blend of poly[4,8-bis[(2-ethylhexyl)oxy]benzo[1,2-b:4,5-b']dithiophene-2,6-diyl][3-fluoro-2-[(2-ethylhexyl)carbonyl] thieno[3,4-b]-thiophenediyl] (PTB7) and [6,6]-phenyl C_{71}-butyric acid methyl ester ($PC_{71}BM$) as the following structure: ITO/PEDOT:PSS (35 nm)/PTB7:$PC_{71}BM$ (100 nm)/PO-TAZ (5 nm)/Al (100 nm) (**Fig. 2c**). The corresponding devices employing pristine Al, LiF/Al, and triphenylphosphine oxide (Ph_3P=O)/Al were also fabricated for comparative study. The current density–voltage (*J–V*) characteristics for typical OSCs based on pristine Al, LiF/Al, Ph_3P=O/Al, and PO-TAZ/Al are shown in **Fig. 2d**. The optimized OSCs with pristine Al electrode gave a power conversion efficiency (PCE) of 4.75%, whereas devices with PO-TAZ yielded a PCE of 7.72%, which is 63.9% higher than the control device (Table 1 and S1, ESI†). Along with enhanced open-circuit voltage (V_{oc}) and short-circuit current (J_{sc}), the fill factor (FF) was found to be 68.81%, which is higher than that of the control device with an FF of 51.79%, resulting from smaller series resistance (R_S) as compared to the control device without PO-TAZ, signifying the effective reduction of the contact resistance (R_c) by formation of an interface dipole between the fullerene derivative and the Al electrode.[15,16] This enhancement is well apparent from the UPS spectra (**Fig. S5,** ESI†), where the secondary cut-off of the PTB7:$PC_{71}BM$ layer with PO-TAZ shifts to the higher energy direction by 0.51 eV, compared with that of only the PTB7:$PC_{71}BM$ layer. This shift is related to the reduction in the vacuum level of the PTB7:$PC_{71}BM$ layer with the PO-TAZ. The dipole layer of PO-TAZ shifts the vacuum level of the adjacent negative electrode layer upwards, leading to better electron transport and extraction when aligned with Al. The PCE of the PO-TAZ-based device is also better than that of OSCs with thermal deposited LiF/Al (PCE = 7.14%). From the structural point of view, both PO-TAZ and Ph_3P=O possess a polar P=O group, which is proposed to modify the ϕ of the cathode by interaction of P=O with Al.[11] The OSCs with PO-TAZ outperform those with Ph_3P=O, owing to higher V_{oc} (0.70 to 0.74 V) and FF (57.71 to

68.81%). Hence, our molecular design strategy of coupling 1,3,5-triazine moiety with P=O group leads to deeper HOMO level (compared to HOMO level of $Ph_3P=O$[17]) and significantly larger interfacial dipoles. The increase in J_{sc} for the PO-TAZ device is further supported by external quantum efficiency (EQE) spectra, which exhibit enhanced light response in the whole 300–800 nm absorption region (**Fig. S6a**, ESI†).

To understand the effect of the PO-TAZ from a topographic perspective, atomic force microscopy was used (**Fig. S7**, ESI†). The pristine PTB7:$PC_{71}BM$ blend on ITO displayed a smooth surface root mean square roughness of 0.92 nm, while the surface of PTB7:$PC_{71}BM$ with PO-TAZ developed a slightly rougher surface (1.42 nm). We also investigated the wetting properties of PTB7:$PC_{71}BM$ and PTB7:$PC_{71}BM$/PO-TAZ films with water (**Fig. S8**, ESI†). The water contact angle of pristine PTB7:$PC_{71}BM$ film was 119° and it was reduced to 92.1° with PO-TAZ and the calculated surface energy showed that PO-TAZ reduced the interfacial tension between the photoactive layer and the electrode (Table S2, ESI†).[18] As a result, we expect better electronic contact between the photoactive layer and the cathode.

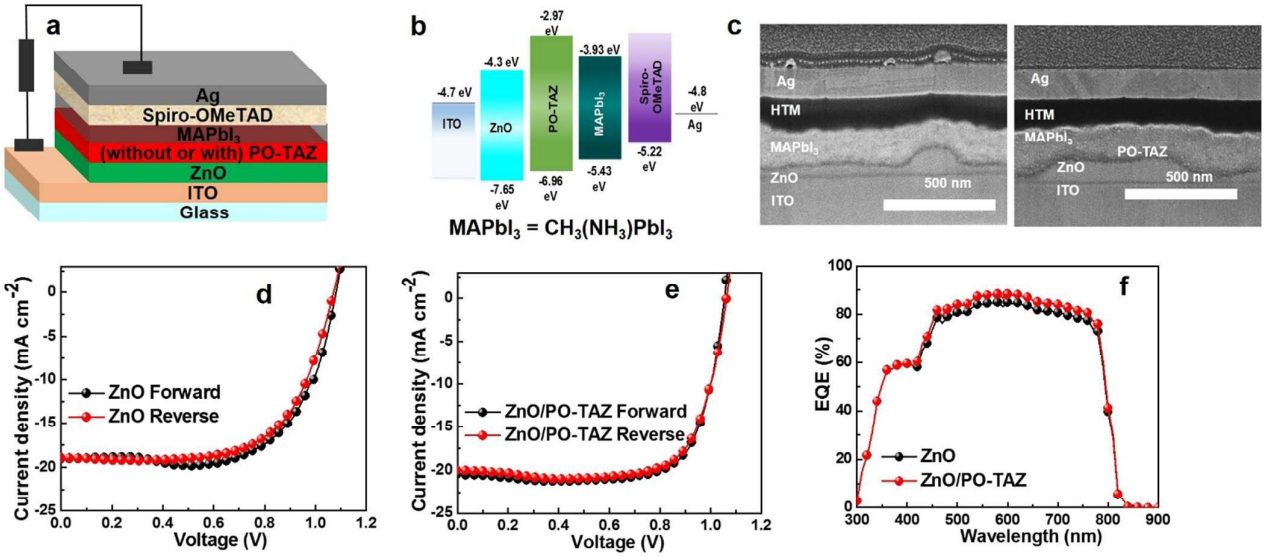

Fig. 3 (a) Device structure; (b) corresponding energy band diagram; (c) cross-sectional SEM image of a representative ITO/ZnO/perovskite ($MAPbI_3$)/without or with PO-TAZ/Ag; (d) *J–V* curves of PSCs without PO-TAZ for the best-performing samples; (e) *J–V* curves of PSCs with PO-TAZ for the best-performing samples; (f) EQE spectra of PSCs without or with PO-TAZ.

2.3. Inverted organic solar cells

To investigate the potential use of PO-TAZ as IL in IOSCs, we fabricated IOSCs with the following configuration: ITO/ZnO (60 nm)/PO-TAZ (5 nm)/PTB7:$PC_{71}BM$ (100 nm)/PEDOT:PSS (10 nm)/Ag (150 nm) (**Fig. 2e**).[19,20] The inverted configuration with ZnO as an electron transport layer was chosen owing to the demonstration of high PCEs in the literature.[21] The IOSCs without PO-TAZ exhibited a maximum PCE of 8.72%, whereas the IOSCs with PO-TAZ showed a maximum PCE of 9.93% (Table 1, **Fig. 2f** and **S6b**, ESI†). To the best of our knowledge, the present PCE results using PTB7 with neutral organic small molecule as IL is among the highest efficiencies of single junction IOSCs reported so far.[22] The beneficial effect of the ZnO/PO-TAZ-based device is that there is accompanied improvement in V_{oc}, J_{sc}, and FF compared to the pristine ZnO-based devices, arising from the significantly improved ϕ shift (**Fig. 1c** and **d**). The shift in ϕ leads to reduced electrostatic potential at the ZnO surface owing to the interfacial dipole created by the interaction between the P=O group of PO-TAZ and the ZnO surface. Thus, the observed linear relationship between ϕ shift and interfacial dipole (i.e., dipole moment) suggests that the ZnO/PO-TAZ is more effective than the pristine ZnO layer (as ZnO also induces interfacial dipole) in charge transport and extraction. The enhanced ϕ shift induced due to PO-TAZ on ZnO layer is well articulated using the working principle as shown in **Fig. S9**, ESI†. As illustrated under flat band conditions, the conduction band of the ZnO layer with PO-TAZ is shifted toward the lower energy direction by 0.4 eV, leading to an increase in V_{BI}, which contributes to the improved V_{oc} (from 0.72 to 0.74 V, Table 1). In addition, the increase in V_{BI} resulting from the introduction of PO-TAZ causes large energy band bending of the photoactive layer under short-circuit conditions (i.e., Fermi levels [E_F] of metal electrodes in metal–organic semiconductor–metal structures are aligned to equilibrium). For the ZnO/PO-TAZ device, the bending of the conduction becomes much steeper than that of the device without PO-TAZ, thus facilitating fast extraction of the photogenerated electrons from the ZnO/PO-TAZ layer compared to that of only the ZnO layer, as supported by the decreased R_S values (from 3.1 to 1.81 Ω cm^2, **Fig. S10**, ESI†) and

thus preventing undesired charge recombination. In addition, the contact angle of water increased from 37.3° (ZnO surface) to 48° (ZnO/PO-TAZ surface). The hydrophobic moieties of PO-TAZ are located on the film surface, whereas the polar group tends to be located near the hydrophilic ZnO (**Fig. S11**, ESI†). Henceforth, ZnO/PO-TAZ forms an intimate interfacial contact with the photoactive layer. It has to be mentioned that even though the PO-TAZ is very thin (5 nm), the PO-TAZ does a lot to improve the PCE of the whole device via improving the electron extraction and transport properties.

To verify the accessibility of PO-TAZ in varying photoactive layers in the device, we fabricated IOSCs using a more prominent narrow band gap polymer, poly[4,8-bis(5-(2-ethylhexyl)thiophen-2-yl)benzo[1,2-b;4,5-b']dithiophene-2,6-diyl-alt-(4-(2-ethylhexyl)-3-fluorothieno[3,4-b]thiophene-)-2-carboxylate-2-6-diyl)] (PTB7-Th) (Table 1 and **Fig. S12**, ESI†). The devices with PO-TAZ showed a much improved PCE of 10.04%, which is higher than that of the device without PO-TAZ (PCE = 8.55%). To analyse the significant effect of PO-TAZ on the electron transport properties of the interlayers, we fabricated electron-only devices containing ZnO and ZnO/PO-TAZ and measured the space charge limited current (SCLC) electron

Table 1 Summary of the photovoltaic performances and parameters for solar cells based on PTB7:$PC_{71}BM$ (conventional and inverted device structures), PTB7-Th:$PC_{71}BM$ (inverted device structure), and conventional $CH_3NH_3PbI_3$ perovskite with or without incorporation of a PO-TAZ, measured under 1,000 W m^{-2} AM 1.5 G illumination.

Photoactive layer (device type)	PO-TAZ	Maximum PCE (%)	Average PCE (%)[e]	J_{sc} (mA cm^{-2})	Integrated J_{sc} (mA cm^{-2})[f]	FF (%)	V_{oc} (V)	R_S (Ω cm^2)
PTB7:$PC_{71}BM$ (Conventional)[a]	No	4.75	4.71	14.12	13.94	51.79	0.65	7.90
PTB7:$PC_{71}BM$ (Conventional)[a]	Yes	7.72	7.64	15.04	14.60	68.81	0.74	2.43
PTB7:$PC_{71}BM$ (Inverted)[b]	No	8.72	8.62	18.11	18.00	65.70	0.72	3.10
PTB7:$PC_{71}BM$ (Inverted)[b]	Yes	9.93	9.66	18.85	18.16	68.85	0.74	1.81
PTB7-Th:$PC_{71}BM$ (Inverted)[a]	No	8.55	8.24	16.42	16.02	65.0	0.80	3.37
PTB7-Th:$PC_{71}BM$ (Inverted)[a]	Yes	10.04	9.77	17.69	17.18	70.0	0.81	2.53
Perovskite (Conventional)[b]	No	13.92[c]	13.60	19.19	19.05	67.26	1.06	3.72
		13.28[d]		18.94	18.19	65.61	1.06	4.10
Perovskite (Conventional)[b]	Yes	16.41[c]	16.23	20.53	19.98	75.92	1.06	1.53
		16.06[d]		20.11	20.01	75.23	1.06	2.24

[a] The photoactive area is 0.09 cm^2. [b] The photoactive area is 0.11 cm^2. [c] Forward direction. [d] Reverse direction. [e] The PCE values are obtained from over 10 devices. [f] J_{sc} from EQE.

mobility ($\mu_{SCLC,e}$). The ZnO/PO-TAZ-based device showed an $\mu_{SCLC,e}$ of 1.32×10^{-4} cm^2 V^{-1} s^{-1}, which is two times higher than the $\mu_{SCLC,e}$ of ZnO with a value of 6.55×10^{-5} cm^2 V^{-1} s^{-1} (**Fig. S13**, ESI†). The mobility results are well aligned with higher FF and the improved dark current (forward bias), as shown in **Fig. S10**, ESI†. The impedance spectroscopy is carried out to study the detailed electrical properties of the PTB7:$PC_{71}BM$ photoactive layer and/or the interface between each layer. The impedance spectroscopy study showed a reduction in the interfacial resistance between the photoactive layer and the ITO electrode (**Fig. S14a**, ESI†). The ZnO/PO-TAZ device has a significantly reduced bulk resistance as seen from the decreased radius in the Nyquist plot. In addition, the lifetimes of the charge carriers are estimated from impedance spectra. The high frequency peak in the Bode plot depicts the charge transfer and the reciprocal of this frequency defines the effective electron lifetime (**Fig. S14b**, ESI†).[23] The electron lifetime of IOSCs with and without PO-TAZ was calculated to be 23.4 and 7.4 μs, respectively, indicating that the device with PO-TAZ undergoes less charge recombination and more efficient carrier transport. We investigated the capacitance (C)–voltage (V) measurements to understand the impact of the insertion of the PO-TAZ layer between the semiconductor and the electrode on the internal electric field in IOSCs.[24] In OSC and IOSC devices, the intrinsic p-doped nature of the semiconducting polymer leads to the formation of a Schottky contact between the electrode and the photoactive layer. The higher doped layers confine the electrical field in the vicinity of the cathode, allowing extraction of the flat-band potential (V_{FB}) and charge carrier concentration. To estimate the V_{FB}, the C–V characteristics were determined by applying a low AC perturbation signal with fixed frequency and sweeping the DC bias and then further examined using the following Mott–Schottky equation: $C^{-2} = 2(V_{FB} - V)/A^2e\varepsilon_r\varepsilon_0N$.[24] Here, V, e, ε_r, ε_0, N, A, and C denote the bias voltage, charge, relative dielectric constant (ε_r = 3), permittivity in vacuum, charge carrier concentration, device active area, and capacitance, respectively. The linear region under low forward bias is related to the formation of a Schottky contact and can be fitted to a plot of C^{-2} versus V. V_{FB} can be evaluated by the extrapolation of C^{-2} = 0 (**Fig. S14c**, ESI†). The extracted V_{FB} is closely related to the V_{BI} for an identical active layer and a positive variation of V_{FB} is the result of an increased V_{BI}.[25] The PO-TAZ/ZnO device shows a higher V_{FB} (0.783 V) compared to 0.741 V of ZnO based device, owing to the lowering of the ϕ of the ZnO layer. This increase in V_{FB} matches the increase in the V_{oc} with PO-TAZ in IOSCs and indicates that the insertion of the new IL induces strengthening of the built-in field, leading to a positive effect on J_{sc} and FF as a result of more efficient charge extraction and reduction of charge recombination. Finally, we examined the long-term stability of non-encapsulated PTB7:$PC_{71}BM$-based IOSCs devices with and without PO-TAZ

stored in air under ambient conditions and their efficiency was measured periodically as shown in **Fig. 2g**.

2.4. Perovskite solar cells

To further prove the generality of this material, we applied PO-TAZ in methylammonium lead iodide ($CH_3NH_3PbI_3$)-based planar PSCs with the configuration: ITO/ZnO (60 nm)/PO-TAZ (5 nm)/ $CH_3NH_3PbI_3$ (250 nm)/Spiro-OMeTAD (200 nm)/Ag (**Fig. 3a**). The same device without PO-TAZ was used as comparison and the energy level diagrams of those components are shown in **Fig. 3b**. The device cross-sectional scanning electron microscope image indicates uniform deposition of layers in PSCs (**Fig. 3c**). Accordingly, the PSCs with ZnO/PO-TAZ showed a significantly improved PCE of 16.41% with an R_S of 1.53 Ω cm^2 and an R_{sh} of 27.1 kΩ cm^2 compared to PSCs without PO-TAZ with a PCE of 13.92%, with an R_S of 3.72 Ω cm^2 and an R_{sh} of 15.5 kΩ cm^2, respectively (**Fig. 3d** and **e**, and **Fig. S15a**, ESI†). The PCE of 16.41% is one of the best efficiencies reported so far for PSCs with planar heterojunction architecture.[26,27] The dramatically higher PCEs of PSCs with PO-TAZ could be ascribed to the improved J_{sc} and FF, which is consistent with the reduced barrier for carrier extraction into the ITO/ZnO electrode. As shown in **Fig. 3f**, the PSCs with PO-TAZ showed a slightly higher EQE maximum of 88.19% at 580 nm than that of PSCs without PO-TAZ of 84.80% at the same wavelength. The reduced R_s and the enhanced R_{sh} indicate that the thin PO-TAZ layer reduces the electronic barrier between $CH_3NH_3PbI_3$ and ZnO layers to improve the photodiode characteristics. To check the reproducibility of device performance, we tested 20 PSC devices that were fabricated with or without PO-TAZ. The PSC devices with PO-TAZ exhibited a high degree of reproducibility in the overall average PCE, when compared to the PSC devices without PO-TAZ (**Fig. S15b** and **c**, ESI†).

Table 2 Fundamental parameters of CNTVT:SVS (9:1), P(NDI2OD-T2), and $PC_{71}BM$ OFETs on Au S/D electrodes with and without PO-TAZ. The characteristics of OFETs were measured with V_D = +60 V. The average mobility of the OFET devices was measured with L = 20 μm and W = 1000 μm.

Semiconductor	Electrodes	Electron mobility (μ_e) (cm^2 V^{-1} s^{-1})	V_{Th} (V)	$I_{on/off}$	R_c (MΩ cm)
CNTVT:SVS (9:1)[a]	Pristine Au	5.6±0.5	40.3	10^2	27.1
CNTVT:SVS (9:1)[a]	PO-TAZ/Au	7.4±0.6	36.8	10^2	15.9
(PNDI2OD-T2)[a]	Pristine Au	0.43±0.01	6.5	10^4	12.6
(PNDI2OD-T2)[a]	PO-TAZ/Au	0.52±0.04	1.4	10^4	5.3
$PC_{71}BM$[a]	Pristine Au	0.07±0.004	4.6	10^3	30
$PC_{71}BM$[a]	PO-TAZ/Au	0.12±0.007	12.8	10^3	17.6
$PC_{71}BM$[b]	Pristine Au	0.004±0.1	18.7	10^3	85.3
$PC_{71}BM$[b]	PO-TAZ/Au	0.03±0.05	4.6	10^3	43.2

[a] Top gate/bottom contact structure. [b] Bottom gate/top contact structure.

2.5. Organic field-effect transistors

To demonstrate the versatile potentials of PO-TAZ for other organic electronic devices, we further investigate PO-TAZ as IL in n-channel OFETs. Typically, n-channel OFETs suffer from the existence of a large electron injection barrier owing to the energetic mismatch between the LUMO of commonly used organic semiconductors and Au source and drain electrodes.[28] Thus n-channel OFETs were fabricated with poly[N,N'-bis(2-octyldodecyl)-naphthalene-1,4:5,8-bis(dicarboximide)-2,6-diyl]-alt-5,5'-(2,2'-bithiophene) [P(NDI2OD-T2)], $PC_{71}BM$, and poly[2,5-bis(2-octyldodecyl)pyrrolo[3,4-c]pyrrole-1,4(2H,5H)-dione-(E)-[2,2-bithiophen]-5-yl)- 3-(thiophen-2-yl)acrylonitrile]-co-selenophene-vinylene-selenophene (CNTVT:SVS, 9:1) (**Fig. 1a**) as n-channel semiconductors and having a top-gate, bottom-contact [TG/BC, architecture = glass/Au (S/D)/semiconductor/PMMA/Au] and a bottom gate, top contact [BG/TC, architecture = $n^{++}Si/SiO_2$/Au (S/D)/semiconductor] structures. **Figs. 4a**, **b**, and **c** display the typical transfer and output characteristics of $PC_{71}BM$, P(NDI2OD-T2), and CNTVT:SVS (9:1) OFETs, respectively. All OFET device parameters are summarized in Table 2, which clearly demonstrate the beneficial effect of employing the PO-TAZ interlayer. Thus, the field-effect electron mobility ($\mu_{FET,e}$) of $PC_{71}BM$, P(NDI2OD-T2), and CNTVT:SVS (9:1) devices Increase by ~ 60%, 300%, and 90% upon Au functionalization with PO-TAZ. For instance, CNTVT:SVS (9:1) OFETs achieve a $\mu_{FET,e}$ of 7.4 ± 0.6 cm^2 V^{-1} s^{-1} (from 5.6 ± 0.5 cm^2 V^{-1} s^{-1}) for a relatively low process temperature (~150 °C).[29,30] The mobility improvement in these OFETs is due to R_c reduction for electron injection by ~ 100% upon PO-TAZ functionalization (Table 2). The effect of PO-TAZ on the OFET performance is almost comparable with other previously reported charge injection layers, such as CsF and PEIE.[31,32] However, the greatest benefits of PO-TAZ are the intrinsic stability of this material, highly improved device stability (*vide infra*) and low temperature processing.

One major issue in n-channel OFETs is the poor ambient and bias stress stability, which mainly results from trap sites concentrated around 3.8 eV owing to hydrated O_2 in air.[33] The

characteristics of P(NDI2OD-T2) and $PC_{71}BM$ OFETs can suffer after exposure to air since these organic semiconductors have borderline LUMO energy (4.0 and 3.7 eV, respectively) for stability to these trap sites. The inefficient charge injection property from Au electrode in n-channel OFETs is another source of the instability. Thus, we also investigated the ambient and operational stability of P(NDI2OD-T2) and $PC_{71}BM$ OFETs with and without PO-TAZ. P(NDI2OD-T2) OFETs with PO-TAZ showed excellent ambient and operational stability (**Fig. 4d** and **e**). The electron mobility of PO-TAZ treated OFETs was almost unchanged after 24 h storage in air. For comparison, the electron mobility of OFETs with pristine Au or CsF treated Au showed more rapid degradation after 120 h. Interestingly, OFETs with a CsF interlayer showed faster degradation than pristine devices even though CsF devices provide better device performance via improved electron injection properties. This is presumably owing to the hygroscopic nature of CsF.[34] After 5 days storage in air, the electron mobility of PO-TAZ treated OFET slightly decreased (<20%), whereas the electron mobility of the CsF treated or

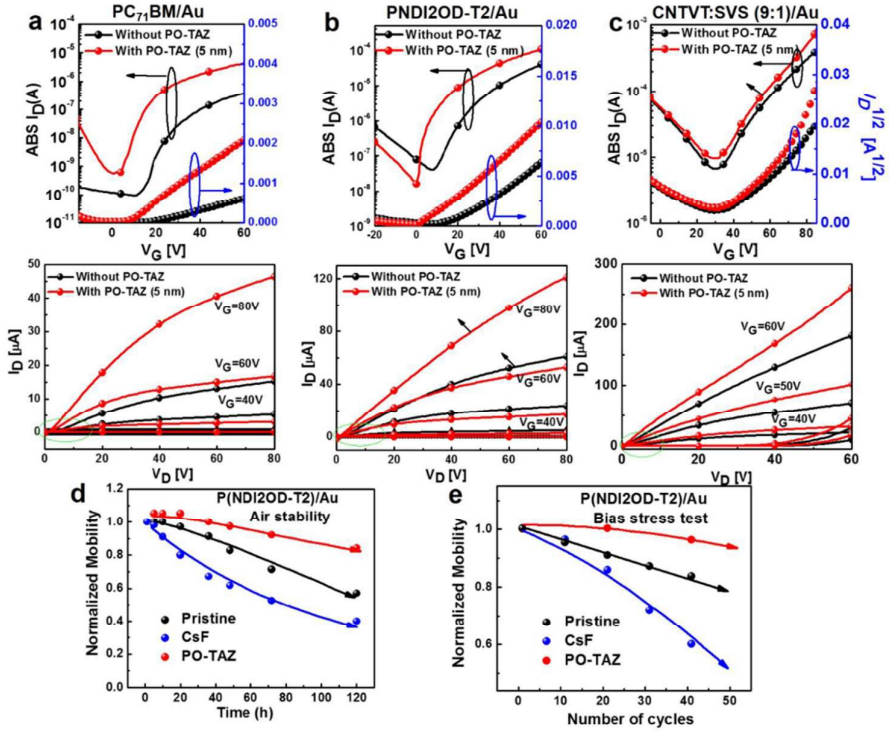

Fig. 4 (a) Transfer and output characteristics of $PC_{71}BM$ OFETs with and without PO-TAZ on Au electrode using bottom gate/top contact structure; (b) transfer and output characteristics of P(NDI2OD-T2) OFETs with and without PO-TAZ on Au electrode using top gate/bottom contact structure; (c) transfer and output characteristics of CNTVT:SVS (9:1) OFETs with and without PO-TAZ on Au electrode using top gate/bottom contact structure; (d) normalized mobility of PO-TAZ treated device compare with pristine P(NDI2OD-T2) and CsF-treated device during air stability test after 5 days; (e) normalized mobility of PO-TAZ treated device compared with pristine P(NDI2OD-T2) and CsF-treated device during 50 cycles scan in bias stress test.

pristine device significantly decreased (45–60%). In addition, P(NDI2OD-T2) OFETs with PO-TAZ exhibit best bias stress stability with only 5% decrease of electron mobility after 50 cycling scans (**Fig. S16**, ESI†). However, OFETs with CsF or pristine Au showed more rapid decrease of electron mobility during the cycling test. We also observed the same trend of ambient and bias stress stability with $PC_{71}BM$ OFETs with PO-TAZ and pristine Au (**Fig. S17**, ESI†). These results indicate that unoptimal contact can accelerate the degradation of these OFETs by generation of joule-heat during the electron injection process.[35]

3. Conclusions

In conclusion, PO-TAZ, a small molecule containing both P=O group and 1,3,5-triazine moiety, was developed and utilized as an IL for various organic electronic devices. The PO-TAZ competency is similar to earlier reported efficient interlayers, with major advantages in easy and simple synthetic design leading to high degree of purity of material combined with the application advantage of both wet coating and vacuum deposition techniques, resulting in reproducibility of device performance and long-term stability. Incorporation of PO-TAZ in organic and perovskite solar cells as well as n-channel OFETs resulted in impressive performance enhancements, which opens the pathway for mass production in large area printing processes. Such high performances in thin film solar cell and OFET devices are achieved by a combination of favourable ϕ

controlling of the electrode and the interfacial modification capability of PO-TAZ. Our findings indicate that P=O-functionalized 1,3,5-triazine derivatives exemplify an exceptional scaffold for interface modification of semiconductors/electrodes in a wide range of optoelectronic devices.

Acknowledgements

This work was supported by a grant funded by the National Research Foundation (NRF) (2011-0028320, 2015M1A2A2056216) by the Ministry of Science, ICT & Future Planning (MSIP) of Korea.

Notes and references

1. R. H. Friend, R. W. Gymer, A. B. Holmes, J. H. Burroughes, R. N. Marks, C. Taliani, D. D. C. Bradley, D. A. Dos Santos, J. L. Brédas, M. Lögdlund and W. R. Salaneck, *Nature,* 1999*,* **397***,* 121-128.
2. G. Yu, J. Gao, J. C. Hummelen, F. Wudl and A. J. Heeger, *Science,* 1995, **270**, 1789-1791.
3. He Yan, Zhihua Chen, Yan Zheng, Christopher Newman, Jordan R. Quinn, Florian Dötz, Marcel Kastler and A. Facchetti, *Nature,* 2009*,* **457**, 679-686.
4. X. Bulliard , S.-G. Ihn, S. Yun, Y. Kim, D. Choi, J.-Y. Choi, M. Kim, M. Sim, J.-H. Park, W. Choi and K. Cho, *Adv. Funct. Mater.,* 2010, **20**, 4381-4387.
5. T. Stubhan, M. Salinas, A. Ebel, F. C. Krebs, A. Hirsch, M. Halik and C. J. Brabec, *Adv. Energy Mater.,* 2012, **2**, 532–535.
6. C.-H. Lin, S. Chattopadhyay, C.-W. Hsu, M.-H. Wu, W.-C. Chen, C.-T. Wu, S.-C. Tseng, J.-S. Hwang, J.-H. Lee, C.-W. Chen, C.-H. Chen, L.-C. Chen and K.-H. Chen, *Adv. Mater.,* 2009*,* **21**, 759-763.
7. Z. He, C. Zhong, S. Su, M. Xu, H. Wu and Y. Cao, *Nat. Photonics,* 2012*,* **6**, 593-597.
8. G. E. Lim, Y. E. Ha, M. Y. Jo, J. Park, Y.-C. Kang and J. H. Kim, *ACS Appl. Mater & Interfaces.* 2013, **5**, 6508-6513.
9. Z. A. Page, Y. Liu, V. V. Duzhko, T. P. Russell and T. Emrick, *Science,* 2014, **346**, 441-444.
10. H. Azimi, T. Ameri, H. Zhang, Y. Hou, C. O. R. Quiroz, J. Mi, M. Hu, Z.-G. Zhang, T. Przybilla, G. J. Matt, E. Spiecker, Y. Li and C. J. Brabec, *Adv. Energy Mater.,* 2015, **5**, 1401692.
11. S. O. Jeon, J.-H. Kim, J. W. Kim, Y. Park and J. Y. Lee, *J. Phys. Chem. C*, 2011, **115**, 18789-18794.
12. W.-Y. Tan, R. Wang, M. Li, G. Liu, P. Chen, X.-C. Li, S.-M. Lu, H. L. Zhu, Q.-M. Peng, X.-H. Zhu, W. Chen, W. C. H. Choy, F. Li, J. Peng and Y. Cao, *Adv. Funct. Mater.,* 2014*,* **24**, 6540-6547.
13. C. Sun, Z. M. Hudson, M. G. Helander, Z.-H. Lu and S. A. Wang, *Organometallics,* 2011, **30**, 5552-5555.
14. J.-W. Kang, D.-S. Lee, H.-D. Park, Y.-S. Park, J. W. Kim, W.-I. Jeong, K.-M. Yoo, K. Go, S.-H. Kim and J.-J. Kim, *J. Mater. Chem.,* 2007, **17**, 3714-3719.
15. V. D. Mihailetchi, P. W. M. Blom, J. C. Hummelen and M. T. Rispens, *J. Appl. Phys.,* 2003, **94**, 6849-6854.
16. C. J. Brabec, A. Cravino, D. Meissner, N. S. Sariciftci, T. Fromherz, M. T. Rispens, L. Sanchez and J. C. Hummelen, *Adv. Funct. Mater.,* 2001*,* **11**, 374-380.
17. S. O. Jeon and J. Y. Lee, *J. Mater. Chem.,* 2012, **22**, 4233-4243.
18. S. Wu, *Journal of Polymer Science Part C: Polymer Symposia* 1971, **34**, 19-30.
19. M. Song, J. H. Park, C. S. Kim, D.-H. Kim, Y.-C. Kang, S.-H. Jin, W.-Y. Jin and J.-W. Kang, *Nano Res*., 2014, **7**, 1370-1379.
20. M. Song, H.-J. Kim, C. S. Kim, J.-H. Jeong, C. Cho, J.-Y. Lee, S.-H. Jin, D.-G. Choi and D.-H. Kim, *J. Mater. Chem. A*. 2015, **3**, 65-70.
21. K. Zhang, C. Zhong, S. Liu, C. Mu, Z. Li, H. Yan, F. Huang and Y. Cao, *ACS Appl. Mater. Interfaces.* 2014*,* **6**, 10429-10435.
22. L. Nian, W. Zhang, N. Zhu, L. Liu, Z. Xie, H. Wu, F. Würthner and Y. Ma, *J. Am. Chem. Soc*., 2015, **137**, 6995-6998.
23. B. J. Leever, C. A. Bailey, T. J. Marks, M. C. Hersam and M. F. Durstock, *Adv. Energy. Mater*., 2012, **2**, 120-128.
24. P. P. Boix, J. Ajuria, I. Etxebarria, R. Pacios, G. Garcia-Belmonte, J. Bisquert, *J. Phys. Chem. Lett.,* 2011**, 2**, 407-411.
25. T. Kirchartz, W. Gong, S. A. Hawks, T. Agostinelli, R. C. I. MacKenzie, Y. Yang, J. Nelson, *J. Phys. Chem. C.,* 2012, **116**, 7672-7680.
26. P. C. Tao, S. Neutzner, L. Colella, S. Marras, A. R. S. Kandada, M. Gandini, M.D. Bastiani, G. Pace, L. Manna, M. Caironi, C. Bertarelli and A. Petrozza, *Energy Environ. Sci.,* 2015, **8**, 2365-2370.
27. D. Liu and T. L. Kelly, *Nat. Photonics,* 2014*,* **8**, 133-138.
28. C. Liu, Y. Xu, Z. Liu, H. N. Tsao, K. Muellen, T. Minari, Y.-Y. Noh and H. Sirringhaus, *Org. Electron.,* 2014*,* **15**, 1884-1889.
29. H. Sirringhaus, P. J. Brown, R. H. Friend, M. M. Nielsen, K. Bechgaard, B. M. W. Langeveld-Voss, A. J. H. Spiering, R. A. J. Janssen, E. W. Meijer, P. Herwig and D. M. de Leeuw, *Nature,* 1999*,* **401**, 685-688.
30. H. Klauk, *Chem. Soc. Rev*., 2010, **39**, 2643-2666.
31. D. Khim, K.-J. Baeg, J. Kim, J.-S. Yeo, M. Kang, P. S. K. Amegadzea, M.-G. Kim, J. Cho, J. H. Lee, D.-Y. Kim and Y.-Y. Noh, *J. Mater. Chem.,* 2012*,* **22**, 16979-16985.
32. Y. Zhou, C. F.-Hernandez, J. Shim, J. Meyer, A. J. Giordano, H. Li, P. Winget, T. Papadopoulos, H. Cheun, J. Kim, M. Fenoll, A. Dindar, W. Haske, E. Najafabadi, T. M. Khan, H. Sojoudi, S. Barlow, S. Graham, J.-L Brédas, S. R. Marder, A. Kahn and B. Kippelen, *Science,* 2012*,* **336**, 327-332.
33. R. Kim, P. S. K. Amegadze, I. Kang, H.-J. Yun, Y.-Y. Noh, S.-K. Kwon and Y.-H. Kim, *Adv. Funct. Mater.,* 2013*,* **23**, 5719-5727.
34. S. Jeon and H. Hwang. *J. Appl. Phys.* 2003, **93**, 6393-6395.
35. H. Sirringhaus, *Adv. Mater*., 2009, **21**, 3859-3873.

Table of Contents Entry

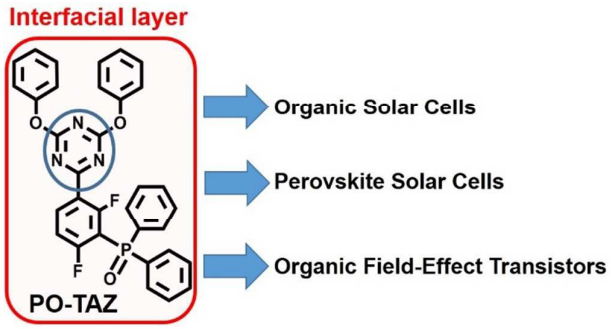

High device performance and stability for various organic electronic devices such as organic, perovskite solar cell and organic field-effect transistor were achieved by incorporation of PO-TAZ as an interfacial layer.

Broader Context

Recently, developing solution-processed stable interfacial layer (IL) is an important topic in the field of organic electronics for high device performance and stability. Even though, various efficient ILs have already been reported, low chemical and ambient stability, intricate synthetic and purification methodologies, poor batch-to-batch reproducibility, and high vacuum-based expensive film deposition processes hinders their compatibility with large-area roll-to-roll processing technology, which is required for low-cost flexible organic electronics. Therefore, it is thus extremely desirable to find efficient IL to avoid aforementioned problems. Here, we report highly efficient and stable various organic electronic devices by introducing a new neutral organic small molecule based on 1,3,5-triazine i.e., PO-TAZ as an IL for the first time. PO-TAZ is easily processible using environmentally friendly solvents, and it exhibit excellent performances in various organic electronic applications such as organic-, organic-inorganic (perovskite) solar cells and organic field-effect transistor devices. PO-TAZ is very simple, possess easy synthesis and cost effective and it can be applicable to other material systems to validate their potential to achieve mile-stone efficiency for the corresponding devices. This work paves a way for realizing high-performance organic electronic devices in the near future.